Proceedings of 8 ICSHMO, Foz do Iguaçu, Brazil, April 24-28, 2006, INPE, p. 651-662.

THE INDIRECT EFFECT OF AEROSOLS OVER THE AMAZON: FROM OBSERVATIONS TO MODELING

Alexandre A. Costa[1]

Fundação Cearense de Meteorologia e Recursos Hídricos, Fortaleza, Brazil

1. INTRODUCTION

It is well known that tmospheric aerosols are a large source of uncertainty in climate change investigation, concerning both their direct and indirect effects. Some authors suggest that changes in the aerosol concentrations and composition may lead to global modifications in cloud optical properties and precipitation formation processes (Ramanathan et al. 2001, Kaufman et al. 2002).

Over tropical regions, such as the Amazon, biomass burning is a major source of aerosols (Kaufman et al. 1998, Artaxo et al. 1998, Artaxo et al. 2002) and cloud microphysics changes in association with smoke aerosols have been demonstrated in modeling studies (Roberts et al. 2003, Costa and Sherwood 2005), satellite retrievals (e.g. Sherwood, 2002), and in-situ measurements (Andreae et al. 2004).

To what extent the microphysics of Amazonian convection is influenced by its dynamics and in turn can influence the larger scales is still unknown. Particularly, to what extent smoke aerosols may control the properties of Amazon convective clouds by reducing the droplet size remains uncertain. In this context, the Large-Scale Biosphere-Atmosphere Experiment in Amazonia – Smoke Aerosols, Clouds, Rainfall and Climate – *Experimento de Microfísica de Nuvens* (LBA-SMOCC-EMfiN!), the cloud microphysics component of the 2002 "dry-to-wet" LBA campaign, aimed to provide *in situ* measurements of cloud microphysics and aerosols to help reduce this uncertainty.

In this paper, I present both previously published and new results from LBA-SMOCC-EMfiN! data analysis as well as results from parcel model and cloud-resolving model simulations using this data set.

[1] Corresponding author address:
Alexandre Araújo Costa
Head, Department of Meteorolgy and Oceanography
Fundação Cearense de Meteorologia e Rec. Hídricos
Av. Rui Barbosa, 1246, Aldeota
Fortaleza-CE, 60115-221, Brazil
E-mail: alex@funceme.br, alexandrearaujoc@gmail.com

2. FIELD CAMPAIGN AND MICROPHYSICS DATA

The instrumented aircraft of the Universidade Estadual do Ceará (UECE), the so-called Avião Laboratório para Pesquisas Atmosféricas (ALPA), is an Embraer Bandeirante, equipped with global positioning system (GPS), static and dynamic pressure, temperature, dewpoint temperature and liquid water sensors, along with a cloud condensation nucleus counter (CCNC), a forward−scattering spectrometer probe (FSSP−100), modified by Droplet Measurements Technology, Inc., and using DMT's SPP-100 package, and two optical array probes (OAP−200X and OAP−200Y). Table 1 shows a list of the instrumentation installed on board ALPA. The flights during the central part of the campaign (from 25 September to 14 October) were usually conducted in coordination with the research aircraft of the Instituto Nacional de Pesquisas Espaciais (INPE), which was equipped with aerosol and trace gas measurement instrumentation (Andreae et al., 2004).

Table 1 –Instrumentation onboard ALPA

Physical Parameter	Sensor(s)
Temperature	Rosemount 102AU1AF
Static Pressure	Rosemount 1201F
Dynamic Pressure	Rosemount 1221F
Latitude, Longitude, Altitude	Garmin GPS
Dew Point Temperature	EG&G 137-C3-S3
Liquid Water	Csiro-King LWC
Aerosols	CCNC UW 83-1
Hydrometeors	FSSP-100/SPP-100, OAP-200X, OAP-200Y

The cloud microphysics campaign consisted of 72 flight hours distributed among 32 flight legs, between 21 September and 18 October 2002 (Figure 1). Flights will be referred to in this paper in the form YYYYMMDD-N (year, month, date and flight number in that date). As pointed out by

Andreae et al. (2004), the aerosol and microphysics measurements were performed under a broad range of environmental conditions, from the "blue ocean" regime (i.e., the clean air masses at the Brazilian coast, in which low CCN number concentrations result in the development of clouds with low droplet concentrations, showing propensity to coalesce rapidly into raindrops) to the "smoky" regime (in which the large aerosol number leads to much higher droplet concentrations and inhibition of warm-rain processes).

Figure 1 - Aircraft trajectories for the 32 flights by the ALPA instrumented aircraft, between 21 September and 18 October, listed in Table 2. Cities are indicated by numbers: 1. Fortaleza, 2. Teresina, 3. Marabá, 4. Alta Floresta, 5. Ji-Paraná, 6. Porto Velho, 7. Vilhena, 8. Rio Branco, 9. Cruzeiro do Sul.

Here, we present a slightly different classification of the observed regimes from that proposed by Andreae et al. (2004). We retain their definitions of the "blue ocean", "green ocean" and the "smoky" (or "polluted" regime). However, in the present work, pyrocumuli are included into the smoky regime, as an extreme case, and a "transitional" regime is added (with properties that are intermediate between the "smoky" and the "green ocean") to account for changes in the microphysical properties of clouds over the Southern Amazon investigated during flights in October. Also, clouds near the coast are distinguished from their counterparts over ocean, since they often receive influence of continental aerosols as well as urban pollution.

Cloud droplet concentration varied by a factor of about 7 from the blue ocean to the polluted environment. Figure 2 shows the droplet concentration as a function of height for several flights, representative of different regimes. The FSSP measurements were used without correcting for coincidence of droplets in the measurement volume, which might have caused undercounting in the highly polluted clouds. Clean environments showed the smallest droplet concentrations, as expected. At the Northeast Brazil coast, the lowest concentrations were found (flight 20021018-1). Despite the possible influence of pollution coming from Fortaleza's urban area, which may account for the occasional occurrence of concentrations around 500 cm^{-3} (as pointed out by Costa et al. 2000), the collision-coalescence process should be efficient in clouds under these conditions. Over western Amazonia (flights 20021005-1 and 20021005-2) droplet concentrations up to ca. 1000 cm^{-3} were found.

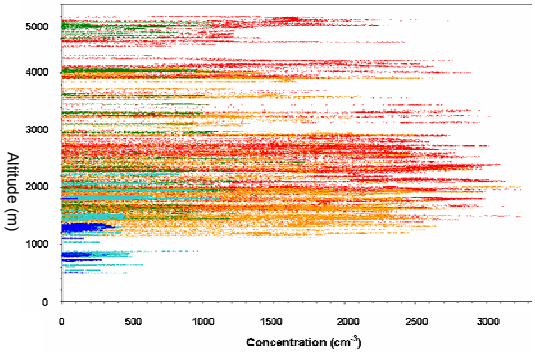

Figure 2 – Droplet concentrations measured by the FSSP in LBA-SMOCC-EMfiN! flights: blue ocean (data collected during flight 20021018-1 over ocean only, in blue), "coastal" clouds (data collected during flight 20021018-1 over land only, in cyan), green ocean (in green), smoky (in red) and transition (in orange).

In polluted air, such as during flights 20020923-1, 20020924-1, 20020926-1, 20020927-1, 20020928-1, 20020930-1, 20020930-2, 20021001-1, and 20021001-2, droplet concentrations are much higher, often approaching 3000 cm^{-3}. Such increased droplet concentrations suggest a significant suppression of precipitation development in the warm phase, since the available water vapor condenses in a large number of very small particles with little chance of coagulation. In fact, it is possible that such concentrations are even larger since, as the number of droplets increase, errors due to coincidence (see, for instance, Brenguier 1989 and Cooper 1988). There are evidences that droplet concentrations inside pyrocumuli actually exceed 4000 cm^{-3}.

The transitional environment generally shows slightly lower droplet concentrations than the polluted one (flights 20021008-1, 20021009-1, 20021011-1, 20021011-2, 20021012-1, 20021013-1, and 20021014-1). Although modest, this reduction may be significant in changing the precipitation efficiency of clouds during that period.

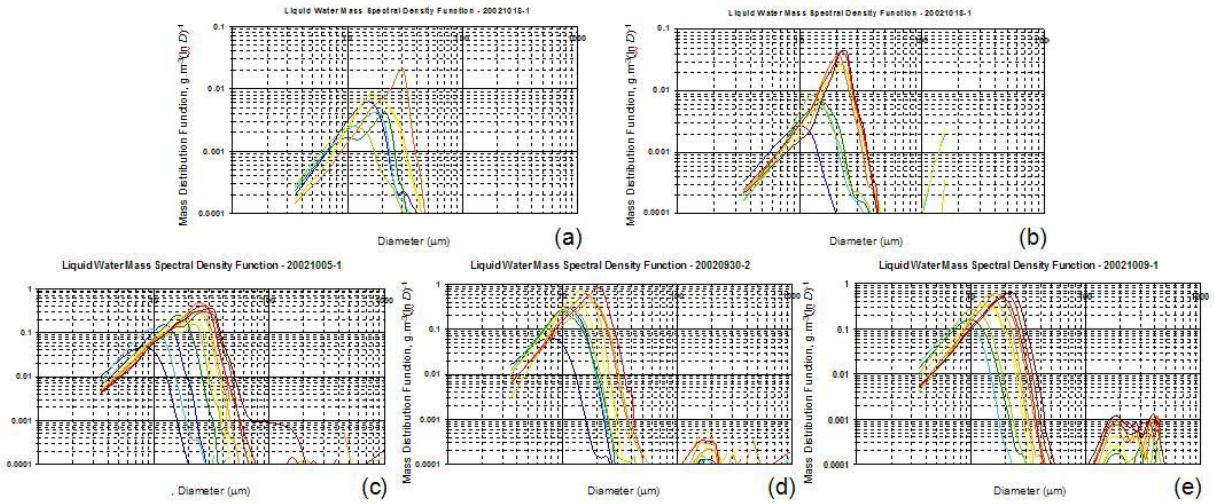

Figure 6 –Mass distributions of hydrometeors for one flight in each of the four regimes. "Warmer" colors indicate higher altitudes. (a) 20021018-1, over ocean (measurements at mean altitudes of 678 m, 725 m, 943 m, 1060 m, 1182 m, 1345 m, and 1710 m), (b) 20021018-1, over land (579 m, 757 m, 1206 m, 1520 m, 1828 m, 1911 m, 1946 m, and 2131 m), (c) 20021005-1 (1452 m, 1615 m, 1926 m, 2307 m, 2945 m, 3110 m, 3379 m, 3598 m, 3914 m, 4038 m, 4663 m, and 4839 m), (d) 20020930-2 (1620 m, 1926 m, 2011 m, 2442 m, 2650 m, 2825 m, 3232 m, 3933 m, 4019 m, 4906 m), (e) 200209-1 (1432 m, 1629 m, 1892 m, 2181 m, 2393 m, 2580 m, 2923 m, 3143 m, 3630 m, 3931 m, 4040 m).

Wide droplet size spectra were found both over the blue and green "oceans", while narrow spectra dominated in polluted environments. Figure 3 shows examples of the distribution of liquid water mass as a function of the droplet diameter, based on data from the FSSP, 200-X and 200-Y probes (in the case of the latter two, data are not being considered as truly quantitative, but as qualitative indicators instead, because of their reduced sample volume and possible water shedding from the probe tips). The spectra are shown in such a way that one can follow the evolution of the droplet distribution evolution with height, and check if there are signs of precipitation development due to collision-coalescence.

Figure 3a corresponds to the observations over the Atlantic Ocean and Figure 3b shows distribution functions of droplets in clouds inland, close to Fortaleza. Wide spectra are present, with a fast increase in the modal diameter, in both cases. This agrees with observations of radar echoes of rain clouds with tops below 3000 m at Fortaleza (Costa et al. 2002). Spectra observed over the "green ocean" show a widening of the distribution function similar to marine conditions. Giant particles apparently do not play a significant role in the "green ocean" air mass, as the set of raindrop-sized particles apparently develops from the "tail" of the droplet spectrum (Figure 3c). This is consistent with the low concentrations of giant nuclei found below cloud base level during the western Amazon flights.

In the polluted environment, the distribution function shows typically two modes (as in Figure 3d): the first, composed of small droplets (modal radius below 10 μm); and the second, of large particles (radius approaching 100 μm). It is noticeable that the small-particle mode does not widen as in the green ocean case, nor is there significant mass growth in the large-particle mode. We believe that because very small particles essentially follow the air flow around a falling large particle, collection of small droplets by the larger particles does not occur and warm rain does not develop.

During the "transition season", aerosol concentrations are still elevated, but slightly less than in the middle of the burning season. Also, more water vapor becomes available at low levels, owing to the change in the large-scale circulation over the Amazon region. As a consequence, cloud base height lowers, raindrop-size particles appear faster and are able to collect the somewhat larger (compared to their counterparts in the smoky environment) droplets that can be present due to the reduced CCN concentration. Some warm rain may

develop in this situation, as suggested in Figure 3e.

3. MODAL LIQUID WATER DIAMETER AND WARM RAIN HEIGHT

As suggested in previous investigations of satellite and radar data analysis (e.g., Rosenfeld 1999), the general effect of pollution on cloud microstructure leads to a reduction of the effective diameter and, consequently, to the inhibition of collision-coalescence. Rosenfeld and Gutman (1994) found that the satellite-retrieved effective diameter (D_{eff}) must reach a value of 28 μm for warm rain initiation. In-situ aircraft measurements show that this satellite-retrieved effective diameter corresponds to a smaller aircraft-retrieved effective diameter for the same height of onset of precipitation (Andreae et al., 2004). This is so probably because aircraft FSSP measurements are truncated, whereas the satellite effective diameter is disproportionably affected by few large hydrometeors (Knyazikhin et al., 2002). Instead of using D_{eff}, Andreae et al. introduced the modal liquid water diameter, D_L, which is not affected by truncation effects. We will call this value the "warm rain threshold" (D_R = 24 μm). The minimum altitude in which $D_L = D_R$ in a developing convective cloud becomes its "warm rain height" (ζ).

Using these definitions, the observed values of D_L, calculated from the distribution function shown previously, have been linearly extrapolated until $D_L = D_R$. With this simple procedure, we evaluate ζ for each flight, representing the altitude at which warm rain formation is probable for a given cloud. An illustration on how this procedure works is shown in Figure 4, in which ζ is calculated for one flight in each regime. The influence of ambient aerosols in determining the development of precipitation in clouds is illustrated in Figure 5. This Figure shows how the warm rain height (determined as in Figure 4) varies as a function of the mean droplet concentration (which is primarily determined by the concentration of CCN) for several LBA-SMOCC-EMfiN! flights (the ones during which the best vertical profiles were collected), as well as the respective cloud base heights. The vertical distance between the cloud base height and ζ is the vertical displacement required, in each case, for a cloud parcel to go from the nucleation of its droplets to the onset of warm rain development via collision-coalescence, or simply its "warm rain depth" (represented by *h*).

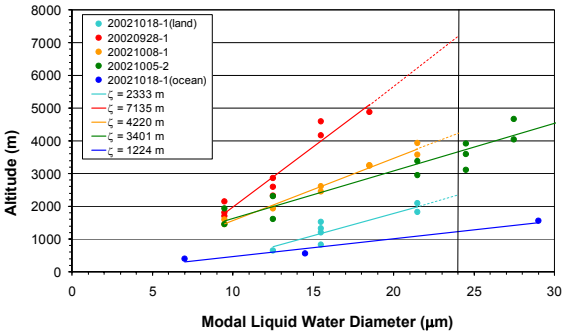

Figure 4 - Effective Diameter as a function of height for four flights: 20020930-2 (polluted), 20021005-2 (green ocean), 20021009-1 (transition) and 20021018-1 (over ocean and over land). The warm rain threshold D_R = 24 μm is indicated by the vertical line. The warm rain height was obtained using a linear regression of the observed values.

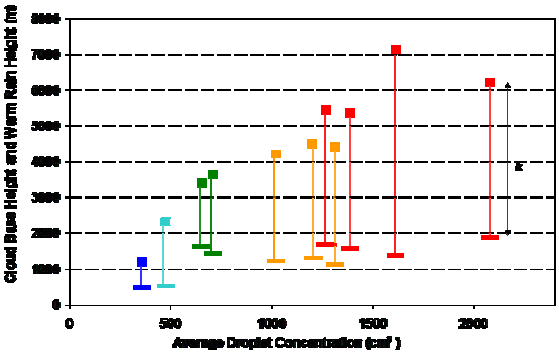

Figure 5 - Warm rain height and cloud base height (in m) as a function of the average droplet concentration (in cm^{-3}) for 10 flights. The various cloud microphysics regimes are represented by different colors: blue ocean (blue), "coastal" clouds (cyan), green ocean (green), smoky (red) and transition (orange). The warm rain depth (*h*) is indicated as the vertical distance between the cloud base and the level of warm rain formation.

Values of ζ ≈ 1200 m (*h* ≈ 700 m) over the ocean and ζ ≈ 2300 m (*h* ≈ 1800 m) over land agree with radar observations in Fortaleza, which show abundant rain development in clouds with tops at or below 3000 m. The value of ζ ≈ 3500 m (*h* ≈ 2000 m) for the green ocean is located well below the freezing level, which again allows warm rain to develop.

Clouds in the transitional regime are apparently in a borderline situation, as the warm

rain height is located near the 0°C isotherm ($\zeta \approx$ 4400 m, $h \approx$ 3200 m). Because supercooled water is a common phenomenon in convective clouds, one might suppose that rain may develop in the warm phase already during the dry-to-wet transition period, due to the increased ability of the population of large particles to collect the smaller droplets. However, further investigation is probably necessary, since at least during the rainy season, Amazon rain clouds tend to glaciate at relatively low altitudes and relatively warm temperatures (about -12 °C, Stith et al. 2002). The question remains if the terminal velocity of liquid-phase particles can overcome the updraft velocity and rainout before reaching the levels at which glaciation takes place.

Finally, in the polluted environment, the droplets grow only to about D_L = 18 μm at the freezing level, well below D_R and are, therefore, far from the onset of precipitation. According to Figure 8, a value of $\zeta \approx$ 5400-7100 m ($h \approx$ 3800-5800 m) is estimated for the smoky clouds. Since drizzle-size particles are carried further up by the updrafts, it is probable that ice-phase processes often start below the height at which their terminal velocity becomes greater than the updraft velocity, and therefore warm rain is inhibited.

Figure 9 depicts the warm rain depth (h) as a function of the droplet concentration, showing that an approximately linear relationship between those two variables might be inferred. As expected and previously discussed by Andreae et al. (2004), smoky clouds must become very deep to reach the onset of warm rain formation, whereas in a clean environment, collision-coalescence is an effective mechanism for producing precipitation in relatively shallow clouds.

4. PARCEL MODEL RESULTS

I used a parcel model to simulate the development of warm rain in different aerosol regimes, from very clean to extremely polluted, as well as to explore sensitivities regarding the presence of giant CCN, the strength of the updraft velocities, and the availability of moisture at the sub-cloud layer. Some of the results shown here were presented in Costa and Sherwood (2005).

The numerical model is a parcel version of Costa et al.'s (2000) two-dimensional model, with explicit microphysics. All major microphysical processes associated with the liquid phase are represented: nucleation, condensation, evaporation, collision-coalescence, collisional and spontaneous breakup.

The model was set to allow up to 167 categories of aerosol particles, according to the specific needs of representing CCN of different sizes (including giant and/or ultra-giant particles). The CCN dry radius ranges from approximately 0.006 to 7.59 μm, corresponding to critical supersaturations of 3.0 % (smallest nuclei) to approximately zero (largest nuclei). Liquid-phase hydrometeors are divided into a set of 100 discrete bins, according to their radius, which varies exponentially from 1 μm to 5 mm. Kogan's (1991) scheme was used to redistribute mass among the discrete bins.

Probabilities of collision, followed by coalescence or breakup are calculated according to Low and List (1982 a, b). Distribution-functions of fragments from filament, sheet and disk collisional breakup are calculated according to Low and List (1982b). As large raindrops are unstable, spontaneous breakup is included, following experimental data from Kamra et al. (1991).

The model is initialized with a cloud-free parcel at a specified temperature, pressure and humidity. The parcel is then forced to ascend at a specified vertical velocity. As the parcel rises, pressure is reduced according to a hydrostatic assumption and its temperature changes due to adiabatic expansion and diabatic release of latent heat due to condensation. Initial conditions correspond to field observations from the LBA-SMOCC-EMfiN! Campaign and encompass different kinds of environment, from the oceanic/coastal type, at northern Northeast Brazil, in which higher dew-point temperatures provide a low lifting condensation level, to the warmer and dryer conditions over central Brazil and southern Amazon, in which cloud bases were predicted and observed at a much higher altitude (Figure 5). Figure 6 shows the range of temperature and dew-point temperatures used to initiate the model. The surface conditions corresponding to the LBA-SMOCC-EMfiN! research flights are represented by small symbols (diamonds, squares, and triangles). The mean values of temperature and dew-point temperature for the different cloud microphysics regimes (smoky, transitional, green ocean and blue ocean) are depicted as big symbols in the same diagram.

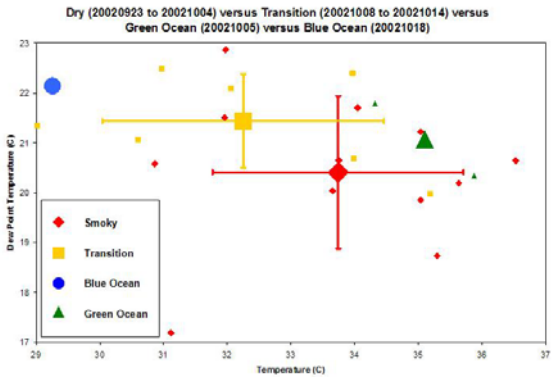

Figure 6 - Observations of temperature and dew-point temperatures from the LBA-SMOCC-EMfiN! campaign. Colors indicate different regimes: smoky (red), transition (orange), "green ocean" (green) and coastal/"blue ocean" (blue). Small symbols represent individual observations, and averages for the different regimes are indicated by large symbols. Error bars indicate standard deviations for the smoky and the transitional regimes.

In order to simulate cloud development, a size-distribution of CCN has to be specified. In most of the simulations, an idealized distribution containing both large aerosols ("common" CCN), giant and ultragiant CCN (UCCN) was used. That "control" distribution was then modified, reducing the concentrations of GCCN and/or UCCN or entirely removing GCCN and/or UCCN. In order to simulate different aerosol concentrations, such distributions were simply multiplied by a factor, which allowed total CCN concentrations to range from 60 cm^{-3} to 60.000 cm^{-3} (at a 3.0 % supersaturation). Such extreme values are meant to represent exceptionally clean environments, such as deep oceanic air masses (lowest concentration) and heavily polluted pyrocumulus formed over forest fires (highest concentration).

I first performed a control run initialized using the relatively dry conditions found during late September 2002 over the polluted, Southeastern, Amazon. We prescribe a vertical velocity of 3 m/s and a control aerosol distribution that includes GCCN and UCCN.

Figure 7 shows the simulated warm rain height (assumed as the minimum altitude at which the modal liquid water diameter reaches a value of D_R = 24μm). Both the model and observations show a general tendency toward increased warm rain height with increased cloud droplet concentration. The predicted warm rain height exhibits an obvious change in behavior when the cloud droplet concentration exceeds ~ 700 cm^{-3}. For concentrations less than this value (i.e., for cleaner environments), the warm rain height increases nonlinearly with CCN concentration. That part of the plot is well explained using very simple arguments on how the available water vapor condenses on a given number of aerosol particles. The adiabatic liquid water content is $q_l = \frac{\pi}{6}\rho_w \overline{D}^3 N$, where ρ_w, N, and $\overline{D}$ represent the density of liquid water, the total hydrometeor number concentration and the mass-averaged diameter $\overline{D} = \left(\frac{1}{N}\int_0^\infty f(D)D^3 dD\right)^{1/3}$ ($f(D)$ is the number distribution-function), respectively. In the absence of coalescence or sedimentation processes, the liquid water content will remain adiabatic and the droplet size distribution will be narrowly distributed about the modal diameter D_R. The warm rain height would occur at $\zeta = F^{-1}\left(\frac{\pi}{6}\rho_w D_R^3 N\right)$, where we assume that $\overline{D}$ equals the threshold modal diameter (D_R). This adiabatic, monomodal estimate is represented by the grey line in Figure 7. It is obvious that such an approximation accounts very well for the behavior of the parcel model in the clean regime.

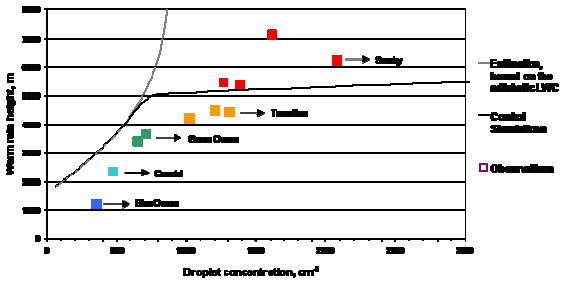

Figure 7 - Observed warm rain height from LBA-SMOCC-EMfiN! observations (symbols), simulated warm rain height values from the parcel model with environmental parameters fixed (dark line), and adiabatic/monomodal estimated warm rain height (pale line), as functions of the droplet concentration. See text for further details.

For droplet concentrations bigger than ~ 800 cm^{-3}, the simulated warm rain height increases at a significantly smaller rate than it does for lower concentrations. This change in behavior keeps the model somewhat close to

observations, while the adiabatic/monomodal calculation obviously departs from reality. The change in behavior arises from the physics of the coalescence processes. Collision and coalescence efficiencies in the model depend on the sizes of both particles involved. Collisions by droplets of similar size are unlikely to coalesce, until their radii approach 25 microns where coalescence quickly becomes efficient. This is the reason for the modal-diameter warm-rain threshold commonly assumed. Collisions by particles of different size are more likely, and can occur even when the larger droplet is too small to coalesce with a droplet of its own size. Thus, colloidal instability may be attained either through sufficient broadening, or through overall enlargement, of the droplet sizes.

In a clean environment, the relatively small population of droplets undergoes sufficiently rapid growth via condensation so that nearly all droplets attain the 24-micron threshold before sufficient broadening has occurred to allow coalescence at smaller modal diameters. Thus, rapid onset of precipitation is predicted at the height indicated by our adiabatic/monomodal calculation. Above a critical CCN concentration, however, sufficient broadening is simulated prior to the attainment of the size threshold to allow "early" coalescence. As further simulations showed (Figure 8), this broadening is greatly facilitated by even miniscule numbers of GCCN/UCCN. The height at which this occurs increases little with further increases in CCN, but is sensitive to GCCN/UCCN, as in Figure 8, which shows that the control (with full GCCN spectra) departs significantly from the case with no GCCN for large concentrations of aerosols and droplets.

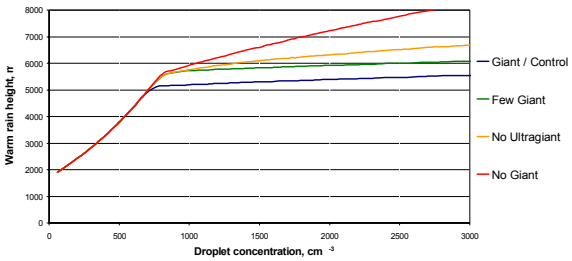

Figure 8 - Simulated warm rain height, as function of the droplet number concentration, for different CCN distributions: control, no UCCN, reduced GCCN/UCCN, and no GCCN/UCCN.

Figures 9 and 10 depict mass distribution-functions for two extreme cases (clean, panel a, versus polluted, panel b) and for simulations with (Figure 9) and without giant CCN (Figure 10). In the clean case, during the condensational growth stage, the mass acquired by the smaller particles is very significant (since there are only few of them to compete for the water vapor) and the mode in the mass distribution-function progresses rapidly, as the small particles tend to catch up with the originally large ones. In contrast, in the polluted case, the raindrop-size particles that appear in upper levels in the simulated cloud (still with fairly low total mass) are able to gain mass via collection of some of the smaller particles (at least the ones that are not so small, so they don't follow the air flow around the collector). The growth of the largest particles via collection is faster than the condensational growth, because of the large number of droplets competing for the water vapor. Because of the presence of the larger CCN that produce those large hydrometeors, the adiabatic assumption fails. In the polluted case, the largest particles (GCCN and UCCN) tend to be very important as precipitation embryos. The no GCCN droplet spectra in a clean environment (panel 10a) are very similar to their counterparts in the control simulation (panel 9a). However, in the polluted, no GCCN simulation, there are no signs of precipitation-size particles (panel 10b), in contrast with the control simulation, in which the presence of GCCN allowed a second mode to appear, in accordance to observations (panel 9b).Those simulations suggest that the most polluted environments are the most sensitive to the presence of giant and ultra-giant particles.

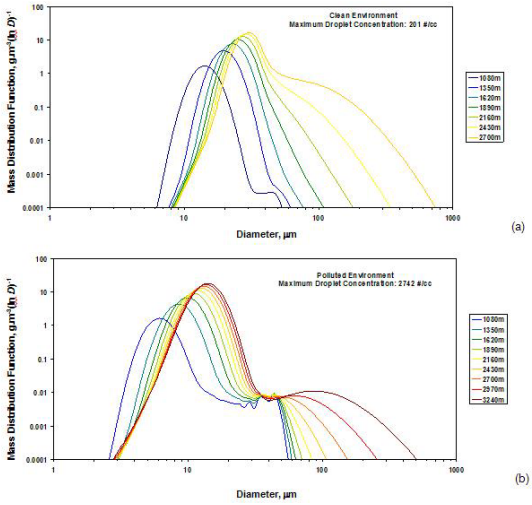

Figure 9 - Mass distribution-functions for two extreme cases (clean, panel a, versus polluted, panel b) in the control set of simulations. Different curves indicate the time evolution of the droplet spectra (which also corresponds to different heights).

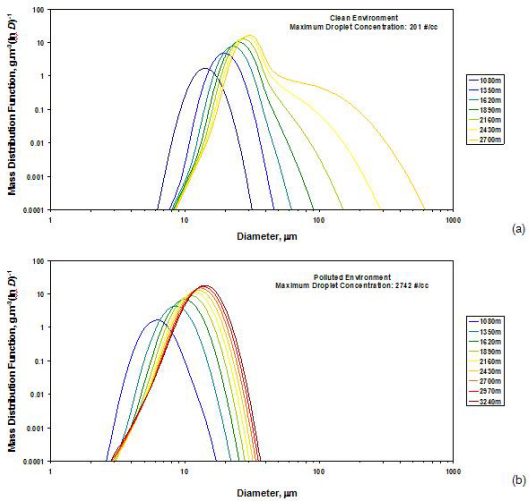

Figure 10 – Same as Figure 9, except for the no GCCN/UCCN simulation.

Parcel model also suggested that other factors such as the in-cloud vertical velocity and the low-level moisture are import to determine the warm rain height.

In order to assess the microphysical sensitivity to the vertical velocity (w), several sets of numerical experiments were performed, in which we prescribed w = 2, 3, 4, and 6 m/s, for the same range of total CCN concentrations as in previous sections and using the control size distribution of aerosols.

The vertical velocity affects microphysical development in two ways. First, w determines the rate at which adiabatic expansion of a cloud parcel produces supersaturation, which in turn controls the number of CCN that are activated.. This well-known effect causes, in our model, roughly a doubling of the maximum droplet number concentration N, going from w = 2 to 8 m/s and holding CCN fixed. Though this affects N, it would not obviously alter the function $\zeta(N)$. Second, a more rapid ascent of the cloud parcel leaves less time for coalescence processes to occur. This should reduce ζ for a given N, but only when N>700 or so and we are in the polluted model regime.

Results shown in Figure 11 confirm that the modeled warm rain height is insensitive to the vertical velocity for low droplet concentrations N, regardless of why N is low. This is not the case for larger N, where ζ increases with N. Given a fixed period of time, the smaller distance traveled by the cloud parcel with a small vertical velocity allows a larger number of collection events to occur, and therefore large droplets originated over the largest CCN are able to reach precipitation-size at lower altitudes, as opposed to the case of strong updrafts.

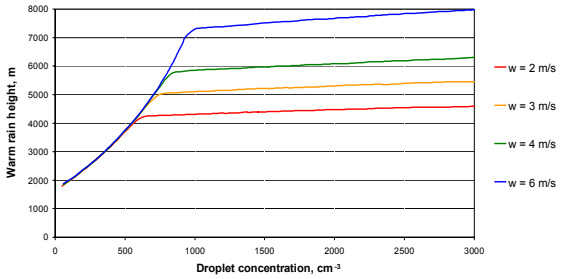

Figure 11 - Same as figure 8, except that vertical velocity is varied.

The most obvious impact of the initial temperature and water vapor mixing ratio in the parcel is in controlling the cloud base height, which should depend on dewpoint depression. In Figure 5, cloud bases were roughly at 500 m over the “blue ocean,” whereas in the polluted and green ocean regimes, cloud bases were much higher (1500 m or more at times). During the transitional regime, the increased low-level dew points led to a reduction in the cloud base height to about 1200 m. These heights were approximately reproduced by the model, in which adiabatic parcels first saturated at at 860 m (blue ocean) 1360 m (transition), 1630 m (polluted), and 1700 m (green ocean).

To explore the sensitivity to temperature and humidity, simulations were performed using the range of temperatures and dew points found during the LBA-SMOCC-EMfiN! campaign (see Fig. 1), keeping the control CCN distribution (i.e., with both GCCN and UCCN included) and a fixed vertical velocity of 3 m/s. The outcome is depicted in Figure 12, which again shows ζ (N) for the various initial parcel states.

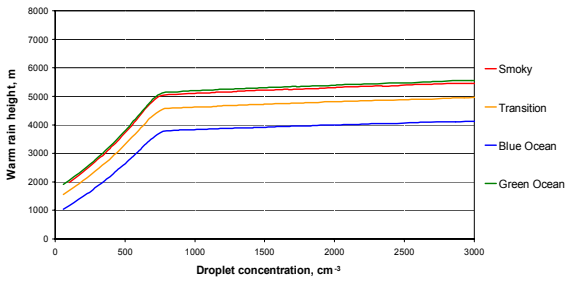

Figure 12 - Same as figure 8, except that initial parcel temperature and humidity is varied (accordingly to Figure 1).

An obvious feature in Figure 12 is that the warm rain height is more sensitive to moisture than is the cloud base height, especially for higher droplet concentrations. For instance, from the polluted to the transition cases, there was a reduction in the simulated cloud base height of 270 m, whereas the warm rain heights differs by more than 500 m at a 2000 cm^{-3} droplet number concentration, with GCCN included. It is clear that this discrepancy increases with *N*. Also, it is larger when GCCN are not present (in the no GCCN simulations, it increases to about 700 m for a 2000 cm^{-3} droplet number concentration).

The fact that subtle changes in the low-level humidity lead to modest variations in the cloud base heights, but more substantial changes in the warm rain height, is associated with the non-linearity of the Clausius-Clapeyron equation, as discussed by Costa and Sherwood (2005).

5. CLOUD-RESOLVING MODEL RESULTS

Cloud-resolving models (CRMs) are regarded as a valid tool to investigate how the cloud system statistics respond to changes in physical parameters. In the present work, I performed long-term cloud-resolving simulations using a large-domain, two-dimensional CRM in order to assess effects of changing cloud microphysics over the larger scales. Specifically two sensitivity runs were carried out, representing a “clean world” and a “polluted world”.

The numerical model was the Regional Atmospheric Modeling System (Pielke et al. 1992), which is non-hydrostatic, fully compressible, with a very comprehensive cloud microphysics package (7 hydrometeor species, represented by generalized gamma distributions) that interacts with the two-stream radiation scheme. 4000 horizontal grid points were used, with a 3km grid-spacing. Cyclic boundary conditions were assumed, along with a non-local nudging for momentum to keep the model domain at rest. The model was initialized with a horizontally homogeneous TOGA-COARE sounding. Two 80-day simulations were performed in which quasi-equilibrium was reached after about 20-25 days. The surface boundary conditions included a SST linear profile (24 to 30 degrees, in order to allow the occurrence of a stable regime over cold waters, characterized by a capped stratocumulus-layer and of a deep convective regime over warm waters, see Figure 13). The two simulations differed in the prescribed droplet concentration: clean (200 cm^{-3}) vs. polluted (2000 cm^{-3}).

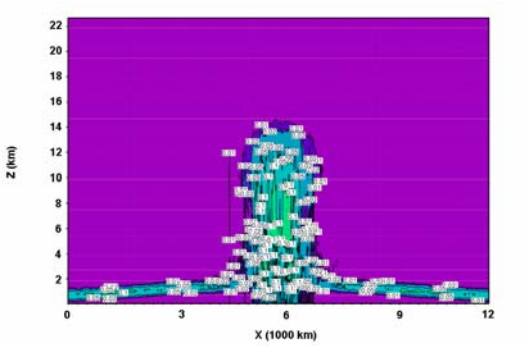

Figure 13 – 60-day average (after quasi-equilibrium is reached) of the condensate (ice plus liquid water) mixing ratio. Deep convective clouds form at the center of the domain (over warm waters), whereas shallow, stratiform clouds are present at the domain sides (over cold waters)

Figure 14 shows that the model indeed reaches a quasi-equilibrium state in each run. In the polluted run, it is noticeable that the quasi-equilibrium average water vapor and condensate mixing ratios are greater than in the clean run.

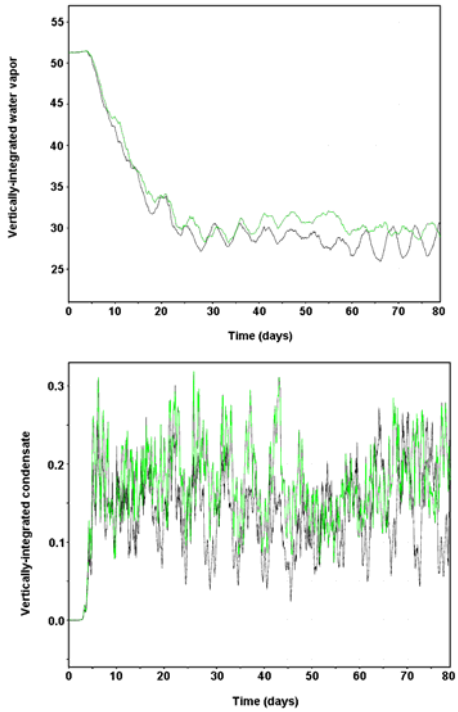

Figure 14 – Evolution of the domain-average, vertically integrated water vapor (upper panel) and condensate (lower panel) mixing ratios. Black lines represent the “clean world” simulation whereas green lines represent the “polluted world” simulations.

One of the most important differences in the two runs concerned the average cloud water mixing ratio, which was much greater in the polluted regime. Considering only the deep convective regime, the total condensate mixing ratio in the polluted run exceeded the one in the clean run by as much as 0.8 g/kg. This accounts for most of the condensate excess in the polluted simulation as depicted in Figure 15. The rainwater mixing ratio is also slightly reduced in the polluted simulation.

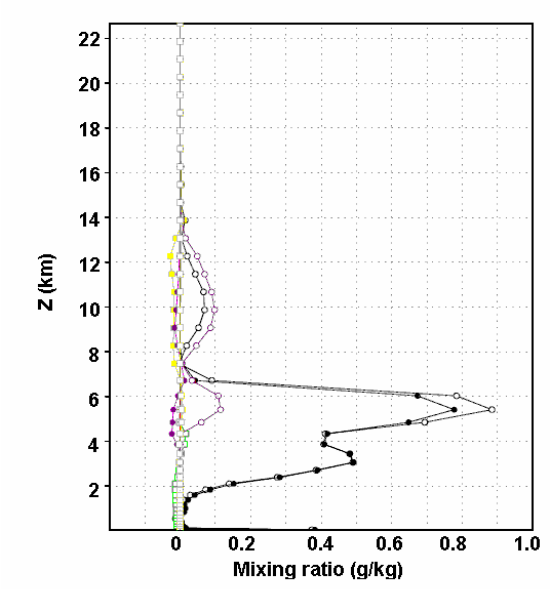

Figure 15 – Differences (polluted minus clean) in the total (black line, closed circles), cloud water (black line, open circles), rainwater (green squares) mixing rations and in the mixing rations for the various classes of ice.

The presence of more water vapor and more cloud water in the polluted run caused a reduction in the shortwave radiative flux at the surface. Feedbacks including a time-evolving surface-temperature, depending on the radiative fluxes are planned.

6. GENERAL DISCUSSION

I have presented cloud microphysics data collected during a field campaign in September and October 2002, focusing on Brazilian Amazonia. Results from model simulations concerning the indirect effect of aerosols were also shown.

Overall, the analyses of observational data confirm the idea that warm rain is strongly inhibited in the polluted environment over parts of Amazonia during the burning season. However, during the transition from the dry to the wet season, which is characterized by increased moisture and reduced aerosol emissions, there appears to be a rapid lowering of the warm rain height (the altitude at which a drop size modal water content of 24 μm is reached). This is caused by a shift to slightly larger droplets (formed in response to smaller CCN concentrations and larger water substance mixing ratios), which are now able to coalesce and to be collected by the large hydrometeors originated from giant and ultragiant aerosol particles. There are remarkable differences between the microphysical properties of clouds over the clean regions of western Amazonia and the smoke-polluted areas in southern Amazonia. Average concentrations of CCN and droplets are larger in the polluted regime by at least a factor of 2. Using typical values for droplet concentrations observed during the wet season from Stith et al. (2002), versus the concentrations we observed in the smoky regime, this factor may even be greater than 6.

From numerical simulations using a simple parcel model, I have argued that simple "Twomey effect" thinking (adiabatic water content distributed over variable droplet numbers) can only apply in clean environments. In polluted environments, our model results indicate that the height for warm precipitation is governed not by overall growth of mean particle size, as is the case in clean environments, but rather by the breadth in the droplet spectrum. In the simulations, collection growth by large particles apparently dominates condensational growth in producing precipitation-size particles in polluted environment. As a consequence, the system becomes sensitive to the presence of giant and ultragiant CCN, since they are responsible for nucleating the larger droplets that might act as collectors. This is not the case in cleaner environments (droplet concentrations below 700-800 cm^{-3}), where GCCN and UCCN are irrelevant for the warm rain development as argued in earlier studies.

The parcel model simulations also indicate that polluted clouds are more sensitive to vertical velocity than clean clouds. In either type the vertical velocity should exert some control in the droplet concentration, as stronger updrafts allow a larger number of CCN to be activated. But in polluted clouds, we find that the warm rain height is further reduced when updrafts are weak, as more collection can occur within a

given altitude range and the larger droplets nucleated over GCCN and UCCN reach precipitation-size at lower altitudes. Therefore, the vertical velocity in a polluted environment might play a double role, with the warm rain height being lowered (elevated) in weaker (stronger) updrafts, due both the activation of a smaller (larger) number of droplets and the increase (decrease) in the number of collision events between the larger hydrometeors nucleated over GCCN/UCCN and other droplets.

I also showed that low-level moisture also appears important in changing the warm rain height, especially when droplet concentrations are large. Predicted warm rain height varies with low-level moisture in the same sense as cloud base height, but with much more sensitivity, because the saturation mixing ratio is a highly non-linear function of temperature (and consequently of height). In polluted environments, subtle variations in boundary layer water vapor mixing ratio might lead to significant variations in the height of warm rain formation. Along with the reduction of the total CCN concentrations, this is possibly an important factor driving the changes in the production of precipitation from the dry to the wet season over the Amazon.

Finally, cloud-resolving simulations suggested that changes in the cloud microphysics may affect global properties of convection. The increase in water vapor and cloud water mixing ratios is particularly noticeable in the CRM results. This suggests that important feedbacks involving the radiation exchange and the surface clouds may also operate. Those should be investigated in further work.

ACKNOWLEDGEMENTS

This paper is in part the result of the compilation of works done along with the SMOCC team and LBA people. Partners such as M. Andreae, D. Rosenfeld, M. A. F. Silva Dias, P. Artaxo and others are deeply acknowledged. I would like to acknowledge the UECE and FUNCEME team that participated in the field campaign and did a superb job in collecting these valuable data. J. B. V. Leal Jr. and G. P. Almeida, from UECE, were partners in developing and adapting the parcel model to simulate the conditions found in the Amazon. I would not forget S. Sherwood from Yale University, which provided me the conditions to continue with this research and is my co-author in publishing the parcel model results.

REFERENCES

Andreae, M. O., D. Rosenfeld, P. Artaxo, A. A. Costa, G. P. Frank, K. M. Longo, and M. A. F. Silva-Dias, 2004: Smoking Rain Clouds over the Amazon. *Science*, **303**, 1337-1342.

Artaxo, P., E. P. Fernandes, J. V. Martins, M. A. Yamasoe, P. V. Hobbs, W. Maenhaut, K. M. Longo, A. Castanho, 1998: Large-scale aerosol source apportionment in Amazonia. *J. Geophys. Res.*, **103**, 31837-31847.

Brenguier, J. L., 1989: Coincidence and dead-time corrections for particle counters. Part II: High concentrationmeasurements with an FSSP. *J. Atmos. Ocean. Techn.*, **6**, 585-598.

Cooper, W. A., 1988: Effects of coincidence on measurements with a forward scattering spectrometer probe. *J.Atmos. Ocean. Techn.*, **5**, 823-832

Costa, A. A., G. P. Almeida, and A. J. C. Sampaio, 2000: A bin-microphysics cloud model with high-order, positive-definite advection. *Atmos. Res.*, **55**, 225-255.

Costa, A. A., Oliveira, J.C.P., Oliveira, C. J., 2002: Estudo de Células Convectivas por Avião-Laboratório e Radar. In: Proceedings of the XII Brazilian Congress of Meteorology, Foz do Iguaçu, Brazil, CD-ROM.

Kamra, A. K., R. V. Bhalwankar, A. B. Sathe, 1991: spontaneous breakup of charged and uncharged water drops freely suspended in a wind-tunnel. *J. Geophys. Res.*, **96**, 17159-17168.

Kaufman, Y. J., P. V. Hobbs, V. W. J. H. Kirchoff, P. Artaxo, L. A. Remer, B. N Holben, M. D. King, D. E. Ward, E. M. Prince, K. M. Longo, L. F. Mattos, C. A. Nobre, J. D. Spinhirne, Q. Ji, A. M. Thompson, J. F. Glason, S. A. Christopher, S. C. Tsay, 1998: Smoke, clouds and radiation – Brazil (SCAR-B) experiment. *J. Geophys. Res.*, **103**, 31783-31808.

Kaufman YJ, Tanre D, Boucher O, 2002: A satellite view of aerosols in the climate system. *Nature*, **419**, 215-223.

Knyazikhin Y., A. Marshak, W. Wiscombe, J. Martonchick, and R. Myneni, 2002: A Missing Solution to the Transport Equation and its Effect on Estimation of Cloud Absorptive Properties. *J. Atmos. Sci.*, **59**, 3572-3585.

Kogan, Y. L.: The simulation of a convective cloud in a 3-d model with explicit microphysics .1. Model description and sensitivity experiments. *J. Atmos. Sci.*, **48**, 1160-1189.

Low, T. B., and R. List, 1982a: Collision, coalescence and breakup of raindrops .1. Experimentally established coalescence efficiencies and fragment size distributions in breakup. *J. Atmos. Sci.*, **39**, 1591-1606.

Low, T. B., and R. List, 1982b: Collision, coalescence and breakup of raindrops . 2. Parameterization of fragment size distributions. *J. Atmos. Sci.*, **39**, 1591-1606.

Ramanathan V, Crutzen PJ, Kiehl JT, Rosenfeld D, 2001: Atmosphere - Aerosols, climate, and the hydrological cycle. *Science*, **294**, 2119-2124.

Rosenfeld, D. and G. Gutman, 1994. Retrieving microphysical properties near the tops of potential rain clouds by multispectral analysis of AVHRR data. *Atmos. Res*. **34**, 259-283.

Rosenfeld, D. 1999. TRMM observed first direct evidence of smoke from forest fires inhibiting rainfall. *Geophys. Res. Letters*, **26**, 3105-3108.

Sherwood, S. C., 2002: Aerosols and ice particle size in tropical cumulonimbus. *J. Climate*, **15**, 1051-1063.

Stith J. L., J. E. Dye, A. Bansemer, A. J. Heymsfield, C. A. Grainger, W. A. Petersen, R. Cifelli, 2002: Microphysical observations of tropical clouds. *J. Appl. Meteor.*, **41**, 97-117